Cell Reports
Medicine

Article

CRISPR-Cas9-mediated deletion of *carbonic anhydrase 2* in the ciliary body to treat glaucoma

Graphical abstract

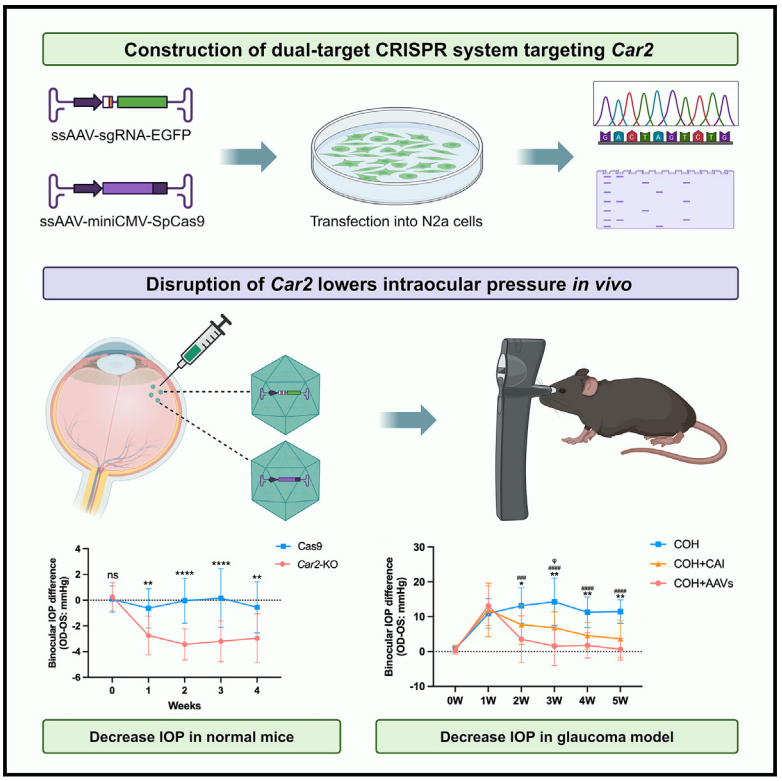

Highlights

- Carbonic anhydrase 2 (*Car2*) gene knockout can reduce intraocular pressure
- Dual-target CRISPR system mediates efficient knockout of *Car2* gene *in vivo*
- A single intravitreal injection can maintain long-term IOP reduction
- CRISPR-Cas9-mediated *Car2* gene knockout as a gene therapy for glaucoma

Authors

Jiaxuan Jiang (蒋嘉烜), Kangjie Kong (孔康杰), Xiuli Fang (方秀丽), ..., Fei Li (李飞), Patrick Yu-Wai-Man, Xiulan Zhang (张秀兰)

Correspondence

lifei.aletheus@gmail.com (F.L.), py237@cam.ac.uk (P.Y.-W.-M.), zhangxl2@mail.sysu.edu.cn (X.Z.)

In brief

Jiang et al. demonstrate that the application of CRISPR-Cas9 technology to disrupt the carbonic anhydrase 2 gene in the eyes can efficiently reduce intraocular pressure, showing promise of achieving the goal of "one-shot treatment, lifelong benefits" for glaucoma.

Jiang et al., 2024, Cell Reports Medicine *5*, 101524
May 21, 2024
https://doi.org/10.1016/j.xcrm.2024.101524

CellPress

Cell Reports Medicine

CellPress
OPEN ACCESS

Article

CRISPR-Cas9-mediated deletion of *carbonic anhydrase 2* in the ciliary body to treat glaucoma

Jiaxuan Jiang (蒋嘉烜),[1,9] Kangjie Kong (孔康杰),[1,9] Xiuli Fang (方秀丽),[1] Deming Wang (汪德明),[1] Yinhang Zhang (张寅航),[1] Peiyuan Wang (王培源),[1] Zefeng Yang (杨泽锋),[1] Yuwei Zhang (张雨薇),[1] Xiaoyi Liu (刘潇逸),[1] Tin Aung,[2,3] Fei Li (李飞),[1,*] Patrick Yu-Wai-Man,[4,5,6,7,8,*] and Xiulan Zhang (张秀兰)[1,10,*]

[1]State Key Laboratory of Ophthalmology, Zhongshan Ophthalmic Center, Sun Yat-sen University, Guangdong Provincial Key Laboratory of Ophthalmology and Visual Science, Guangdong Provincial Clinical Research Center for Ocular Disease, Guangzhou 510060, China
[2]Singapore Eye Research Institute and Singapore National Eye Centre, Singapore, Singapore
[3]National University of Singapore, Singapore, Singapore
[4]Cambridge Centre for Brain Repair, Department of Clinical Neurosciences, University of Cambridge, Cambridge, UK
[5]MRC Mitochondrial Biology Unit, Department of Clinical Neurosciences, University of Cambridge, Cambridge, UK
[6]Cambridge Eye Unit, Addenbrooke's Hospital, Cambridge University Hospitals, Cambridge, UK
[7]Moorfields Eye Hospital, London, UK
[8]UCL Institute of Ophthalmology, University College London, London, UK
[9]These authors contributed equally
[10]Lead contact
*Correspondence: lifei.aletheus@gmail.com (F.L.), py237@cam.ac.uk (P.Y.-W.-M.), zhangxl2@mail.sysu.edu.cn (X.Z.)
https://doi.org/10.1016/j.xcrm.2024.101524

SUMMARY

The carbonic anhydrase 2 (*Car2*) gene encodes the primary isoenzyme responsible for aqueous humor (AH) production and plays a major role in the regulation of intraocular pressure (IOP). The CRISPR-Cas9 system, based on the ShH10 adenovirus-associated virus, can efficiently disrupt the *Car2* gene in the ciliary body. With a single intravitreal injection, *Car2* knockout can significantly and sustainably reduce IOP in both normal mice and glaucoma models by inhibiting AH production. Furthermore, it effectively delays and even halts glaucomatous damage induced by prolonged high IOP in a chronic ocular hypertension model, surpassing the efficacy of clinically available carbonic anhydrase inhibitors such as brinzolamide. The clinical application of CRISPR-Cas9 based disruption of *Car2* is an attractive therapeutic strategy that could bring additional benefits to patients with glaucoma.

INTRODUCTION

Glaucoma is a multifactorial disease characterized by the progressive apoptotic degeneration of retinal ganglion cells (RGCs) and corresponding vision loss, a leading cause of irreversible blindness worldwide.[1] Elevated intraocular pressure (IOP) is considered the sole modifiable risk factor for glaucoma, and lowering IOP is the only clinically proven approach to halt or slow the progression of glaucoma.[2] Generally, the IOP maintains a dynamic equilibrium through aqueous humor (AH) production and flow, outflow resistance, and episcleral venous pressure.[3] Therefore, the primary mechanisms for reducing IOP pharmacologically include suppressing AH secretion and increasing the outflow facility.[4]

Carbonic anhydrase inhibitors (CAIs) are among the oldest IOP-lowering agents used in the management of glaucoma, decreasing AH production from the ciliary body by inhibiting the interconversion of carbon dioxide and carbonic acid.[5] Topical CAIs, such as dorzolamide and brinzolamide, can penetrate the cornea and ocular milieu, reaching the ciliary processes and exerting an IOP-lowering efficacy.[6,7] Previous studies have demonstrated that the ocular hypotensive effect of topical CAIs is mainly through the inhibition of the carbonic anhydrase isoforms 2, 4, and 12,[8–10] with carbonic anhydrase 2 (*Car2*) being the major isoenzyme regulating AH secretion.[11,12] However, topical therapy can be problematic due to noncompliance, low bioavailability, and side effects.[13,14] There is currently no indication that new CAIs that address these issues are being developed.[15,16]

Given that glaucoma is a chronic condition requiring lifelong management, daily anti-glaucoma drug therapy and combined therapies with multiple dosing are the norm in clinical practice.[17] There is, therefore, an urgent need to develop a convenient, effective, and sustained approach for the long-term treatment of patients with glaucoma.[18,19] Gene therapy is being considered for glaucoma due to the eye's relative ease of access and immune privilege, offering a novel and promising therapeutic approach by modifying gene expression.[20,21] Several potential targets for improving glaucoma therapy include increasing AH outflow, decreasing AH production, and promoting RGC neuroprotection and neuroregeneration.[18]

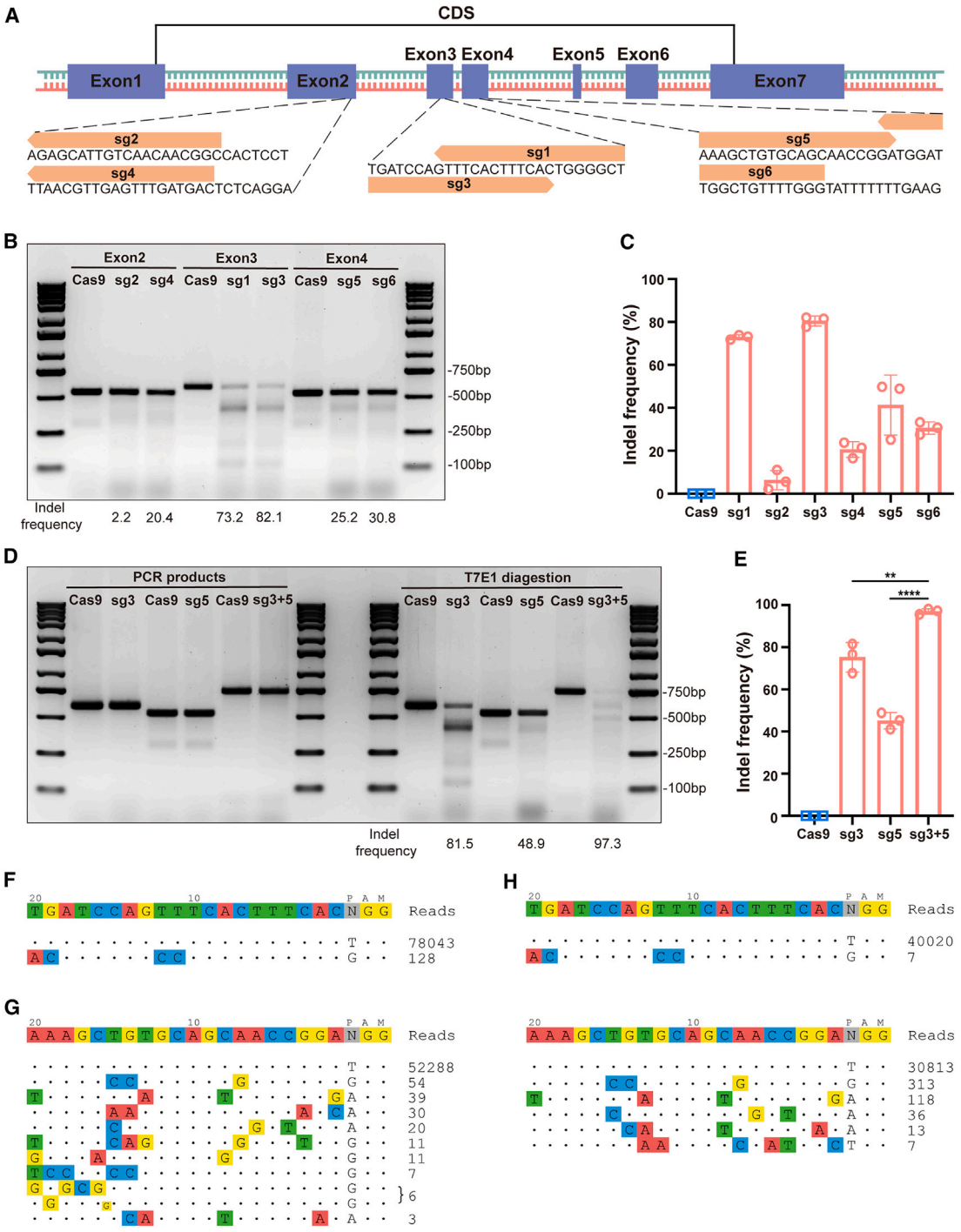

Figure 1. Construction of an efficient dual-target CRISPR system targeting *Car2*

(A) Six candidate sgRNAs targeted the sequences of exons 2, 3, and 4 of the *Car2* gene. CDS, coding sequence; Sg, single guide RNA.

(B and C) The T7E1 assay was employed to evaluate the gene editing efficiency of six sgRNAs transfected in N2a cells individually, with SpCas9 serving as control. Error bars indicate SEM.

(D) Left: the PCR products of the genomic DNA after transfection with individual sgRNA and co-transfection with sgRNA3 and sgRNA5. Right: the bands after digestion with the T7E1 enzyme.

(E) The T7E1 assay showed a higher indel efficiency of 97.3% when combined with sgRNA3 and sgRNA5. Error bars indicate SEM. $^{**}p < 0.01$, $^{****}p < 0.0001$.

(F–H) Off-target potential was assessed using GUIDE-seq analysis. Plasmids were transfected into N2a cells to express SpCas9 and either individual (sgRNA3 or sgRNA5) or paired (sgRNA3 and sgRNA5) gRNAs.

(legend continued on next page)

The CRISPR-Cas9 system has emerged as a promising genome editing tool in the management of glaucoma.[22] Such a system has been used to disrupt the mutant *myocilin* gene and its function in trabecular meshwork cells, which could help prevent further glaucomatous damage in *myocilin*-associated primary open-angle glaucoma.[23] Additionally, when combined with the adenovirus-associated virus (AAV) vector ShH10 serotype, CRISPR-Cas9 could specifically target and edit the *aquaporin 1* gene in the ciliary body, demonstrating an IOP-lowering effect in experimental glaucoma by reducing AH production.[24] To date, there have been no studies exploring the possibility of using CRISPR-Cas9 to target *Car2* for gene therapy of glaucoma. Instead, the major contributions in terms of patent literature have focused on developing pharmaceutical formulations of CAIs.[15,25,26]

In this study, we generated a CRISPR-Cas9 system based on the ShH10 serotype that targets the *Car2* gene in the ciliary body and investigated its IOP-lowering effect in normal mice and experimental glaucoma models. Since the target specificity (off-target effects) and gene editing efficiency are still major challenges for the clinical application of CRISPR-Cas9 technology,[27] dual single guide RNA (sgRNA) directed gene deletion was introduced in our CRISPR-Cas9 system, which has proven to be a more powerful strategy for gene disruption.[28,29] To our knowledge, our study is the first to propose a gene therapy approach targeting *Car2* for the treatment of glaucoma. The clinical translation of CRISPR-Cas9-mediated *Car2* deletion could prove to be a major step change from the traditional use of topical CAIs, with potential additional benefits for patients with various types of glaucoma.

RESULTS

Construction of an efficient dual-target CRISPR system targeting *Car2*

Six candidate sgRNAs targeting exons 2, 3, and 4 of the mouse *Car2* gene were designed (Figure 1A) and cloned into a single-stranded AAV (ssAAV) vector with the enhanced green fluorescent protein (EGFP) as reporter gene. The ssAAV vector plasmid expressing SpCas9 driven by the miniCMV promoter was co-transfected into N2a cells. After sorting EGFP-positive cells (as shown in Figures S1A–S1D), genomic DNA was extracted, and Sanger sequencing revealed pronounced mutations in samples treated with sgRNA3 and sgRNA5, while samples treated with sgRNAs 1, 2, 4, and 6 displayed weaker mutation signals (Figure S1E). The cleavage efficiency of each sgRNA was estimated by T7 endonuclease I (T7E1) assay, demonstrating that sgRNA1–sgRNA6 have average cleavage efficiencies of 72.9%, 6.3%, 80.5%, 20.6%, 41.3% and 30.6%, respectively (Figures 1B and 1C). The analysis of insertion or deletion (indel) profiles indicated that a majority of the variants induced by CRISPR technology were characterized as deletions, with the 1-bp deletion being the most frequently observed (Figures S1F and S1G).

Consequently, we incorporated sgRNA3 and sgRNA5 into an ssAAV vector to maximize the editing efficacy. Analysis using the T7E1 assay demonstrated that the dual-target CRISPR system exhibited an impressive editing efficiency of approximately 97.3% (Figure 1D), which displayed a significant deviation from the results obtained with single-target knockout approaches (Figure 1E). Genome-wide, unbiased identification of double-stranded breaks enabled by sequencing (GUIDE-seq) analysis was used to determine off-target activity. N2a cells were transfected with plasmids carrying spCas9 and either sgRNA3, sgRNA5, or both. sgRNA3 had a single off-target site with a rate of 0.16% (Figure 1F), while sgRNA5 had several sites with a total rate of 0.34% (Figure 1G). Combining sgRNA3 and sgRNA5 did not result in greater off-target effects, with a combined rate of 0.70% (Figure 1H). These findings validated the successful development of an efficient dual-target gene editing system targeting the *Car2* gene.

Efficient knockout of *Car2* reduces IOP in normal mice

The ssAAV vector plasmid expressing sgRNA3 and sgRNA5 was generated and recombined with a ShH10 serotype capsid, which could effectively transfect the non-pigmented epithelial cells (NPECs) of the ciliary body. Meanwhile, the ssAAV-miniCMV-SpCas9 plasmid was packaged in the ShH10 serotype capsid to facilitate the highly efficient dual-target CRISPR system.

To elucidate the impact of *Car2* knockout on IOP, we conducted rigorous binocular measurements of IOP at regular intervals subsequent to the unilateral intravitreal administration of two ShH10-based AAVs at a 1:1 ratio or AAV expressing spCas9 alone (Figure 2A). Importantly, a persistent reduction in IOP was observed post injection in the *Car2* knockout (KO) group, with binocular IOP difference being about 3 mm Hg lower than that of the Cas9 group (Figure 2B; Table S1). A subset of the *Car2* KO group mice was kept for further observation of the long-term effects on reducing IOP, indicating that *Car2* KO could sustainably decrease IOP for up to two months (Figure 2C). Careful isolation of the ciliary body was performed at the fourth week following the surgical procedures (Figure S2), and the genomic DNA extraction solution was subjected to amplification and digestion with T7E1, revealing an average editing efficiency of 92.3% (Figure 2D). To quantify the expression of CAR2 protein, the recently developed ProteinSimple capillary electrophoresis immunoassay was performed, showing a significant reduction of CAR2 protein in the ciliary body of *Car2* KO group (Figures 2E and 2F). Furthermore, the immunofluorescence (IF) imaging consistently demonstrated robust EGFP expression and diminished CAR2 expression in the NPECs (Figure 2G).

Safety evaluation of AAV-mediated *Car2* knockout in mice

To evaluate potential immunogenic or inflammatory responses elicited by intravitreal injections of the AAV, a comprehensive set of investigative assays, including hematoxylin and eosin

(F) sgRNA3 has only one off-target site, with an off-target rate of approximately 0.16%.
(G) sgRNA5 has multiple potential off-target sites, with a total off-target rate of approximately 0.34%.
(H) Co-transfection of sgRNA3 and sgRNA5 did not result in a significant increase in off-target sites, with a total off-target rate of approximately 0.70%.
See also Figure S1.

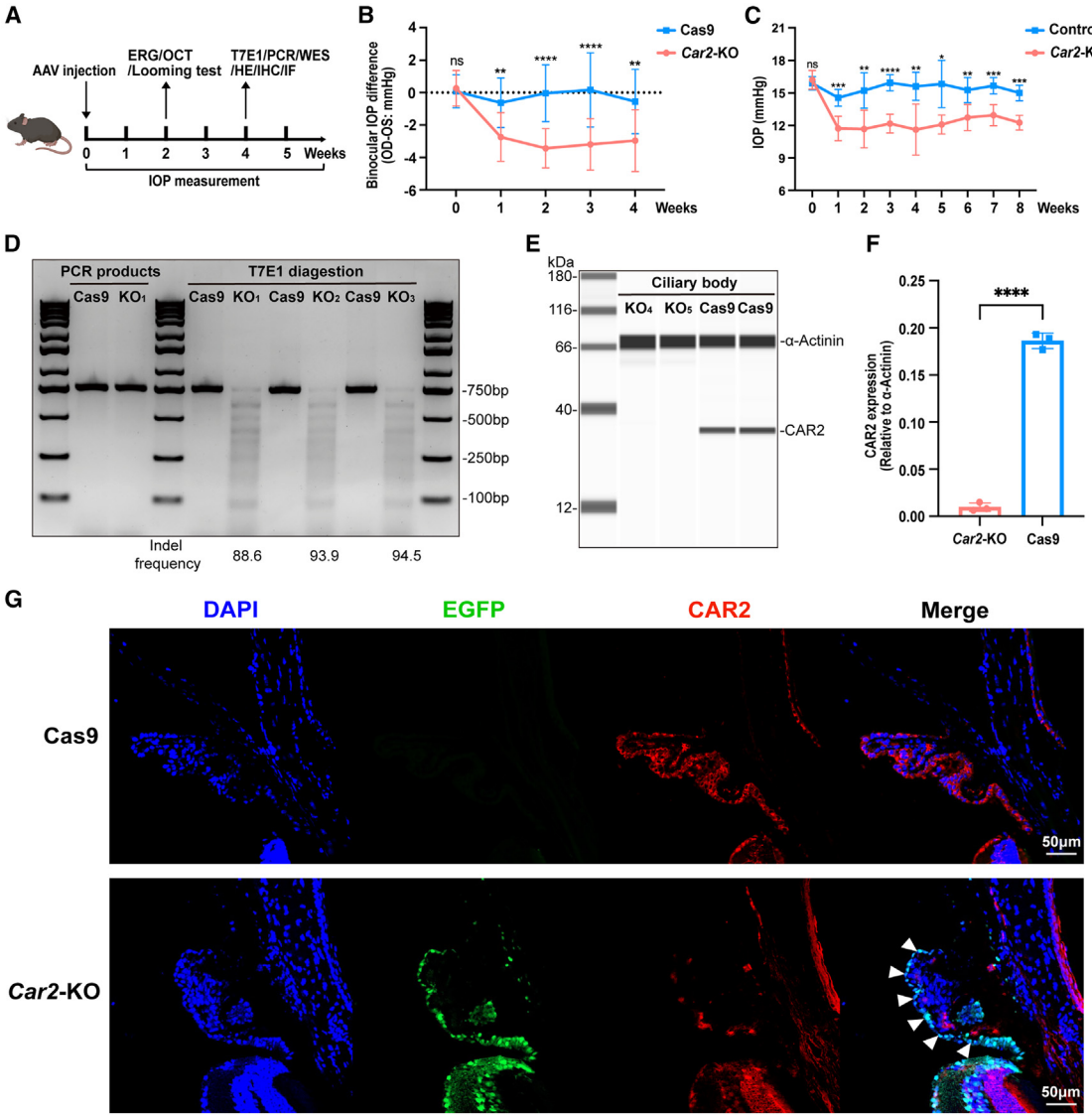

Figure 2. Efficient KO of *Car2* reduces IOP in normal mice

(A) Experimental procedure diagram illustrating the weekly monitoring of IOP following AAV injection, with functional assessments including ERG, OCT, and behavioral assessments of the looming test conducted in the second week. After a comprehensive observation period of 4 weeks, tissue samples were collected for histological examinations, including T7E1, PCR, WES, H&E staining, IHC, and IF. AAV, adenovirus-associated virus; IOP, intraocular pressure; ERG, electroretinography; OCT, optical coherence tomography; WES,; H&E, hematoxylin and eosin; IHC, immunohistochemistry; IF, immunofluorescence.

(B) 12 mice of the Cas9 group were injected with the AAV expressing SpCas9, and 36 mice of the *Car2*-KO group received AAVs expressing both SpCas9 and dual sgRNAs. Binocular IOP difference was recorded for analysis, indicating that the IOP in the *Car2*-KO group is significantly lower compared to the Cas9 group. Error bars indicate SEM. $^{**}p < 0.01$, $^{****}p < 0.0001$. ns, no significance.

(C) Long-term monitoring of IOP in 6 mice of *Car2*-KO group revealed that, compared to the contralateral eyes used as controls, disrupting *Car2* can continuously lower IOP for up to 2 months. Error bars indicate SEM. $^{*}p < 0.05$, $^{**}p < 0.01$, $^{***}p < 0.001$, $^{****}p < 0.0001$.

(D) Evaluation of the gene editing efficiency of the dual-target CRISPR system using the T7E1 assay (3 mice per group).

(E and F) Expression and quantitative levels of *Car2* protein in the ciliary body were examined by WES (3 mice per group). Error bars indicate SEM. $^{****}p < 0.0001$.

(G) Expression of EGFP and *Car2* in the ciliary body was detected under fluorescent microscopy. The white arrows indicate that, in the ciliary NPECs of the *Car2*-KO group, there is significant EGFP fluorescence expression, while the expression of *Car2* is markedly reduced or even absent (3 mice per group).

See also Figures S2 and S3.

(H&E) staining, quantitative real-time polymerase chain reaction (real-time qPCR), immunohistochemistry (IHC), and IF, were used to assess the contralateral untreated eyes of *Car2* KO mice, which were designated as the control group. Pathological assessment revealed no discernible morphological aberrations in the cornea, ciliary body, or retinal structures of the *Car2* KO group when compared with the control group (Figure 3A). The qPCR analyses did not manifest any statistically

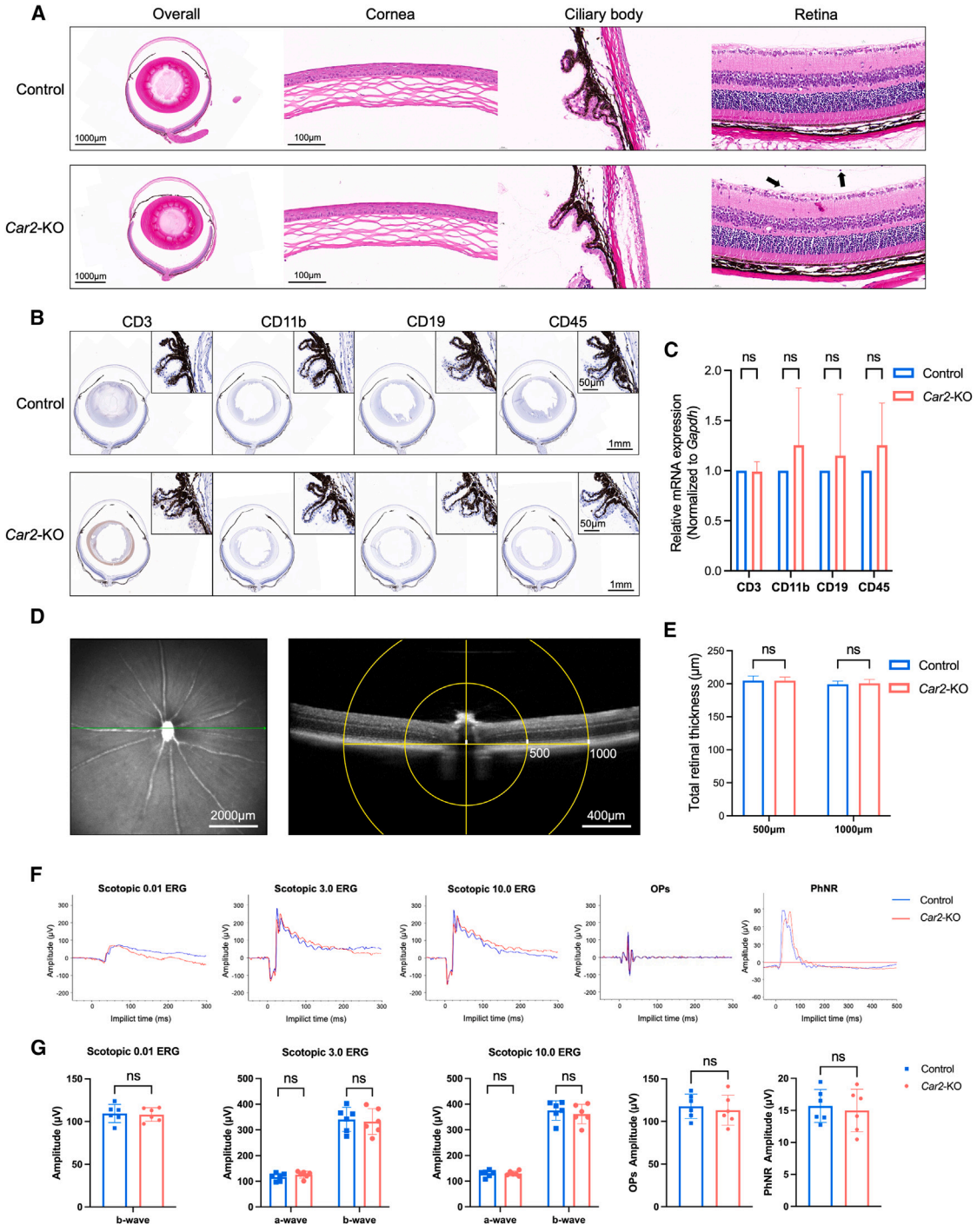

Figure 3. Evaluation of potential side effects caused by *Car2* KO

(A) H&E staining of the overall eyeballs, cornea, ciliary body, and retina of the control and *Car2* KO groups (6 eyes per group). Pathological analysis indicated that a small number of cells shedding (black arrows) in the *Car2* KO group's retina are visible.

(B) IHC staining results suggested that there is no significant immune cell infiltration observed in the ciliary body of the *Car2* KO group mice (3 eyes per group).

(C) The qPCR quantification was performed to assess the expression of immune and monocyte markers (CD3, CD11b, CD19, and CD45) on the ciliary bodies of the *Car2* KO group and the control group (3 eyes per group). Error bars indicate SEM.

(D) OCT imaging was used to visualize the retina, and the total retinal thickness was quantified at points 500 μm and 1,000 μm from the center.

(legend continued on next page)

significant variance in the expression levels of immune cell markers, including CD3, CD11b, CD19, and CD45, in the ciliary bodies of the *Car2* KO mice (Figure 3C), findings that were corroborated by IHC staining (Figure 3B). Considering that the ShH10-based AAV inevitably transfects the retina and reduces CAR2 protein but not the cornea (Figure S3), optical coherence tomography (OCT) examination showed no significant alternations in retinal thickness between the control and *Car2* KO group (Figures 3D and 3E). The glial fibrillary acidic protein labeling did not reveal significant astrocyte activation following AAV transduction when compared to the control group (Figure S4A). Additionally, we performed a scotopic electroretinography (ERG), oscillatory potential (OP), and photopic-negative response (PhNR) tests to evaluate visual functionality in mice. Representative graphs and statistical analysis revealed no significant differences between the two groups, indicating that *Car2* KO does not impair visual functionality in the retina (Figures 3F and 3G). The response of mice to a looming visual stimulus was evaluated and showed that both wild-type mice and *Car2*-KO mice froze and sought shelter immediately upon perceiving an impending stimulus (Figures S4B–S4E). To investigate the long-term effects of viral infection and *Car2* KO on the retina, we conducted OCT examinations and ERG assessments at week 8 and found that no adverse events had occurred (Figures S4F–S4I).

Disruption of *Car2* lowers IOP in a spontaneous glaucoma model

To explore the therapeutic effects of dual-target CRISPR system-mediated KO of *Car2* in glaucoma, we established a breeding colony of DBA/2J mice obtained from Jackson Laboratory, which is a widely recognized model for spontaneous glaucoma (Figure 4A). Regular monitoring of IOP revealed a gradual elevation of IOP in DBA/2J mice compared to C57 mice at the fifth month, with a more pronounced disparity observed at the eighth and ninth months (Figure 4B), resulting in an average IOP difference of 6–11 mm Hg (Table S2). To accentuate the therapeutic efficacy of *Car2* KO, a subset of DBA/2J mice at the ninth month underwent ERG testing to confirm the presence of glaucoma, followed by intravitreal injection of AAVs. Figures 4C and 4D demonstrated a significant reduction in b-wave amplitudes across multiple stimulus thresholds in mice at the ninth month compared to those at the fifth month, accompanied by noticeable attenuation of OPs and PhNR, indicative of compromised visual function. Subsequent to *Car2* KO, weekly monitoring of IOP exhibited a substantial decrease (Figure 4E), and protein analysis of ciliary bodies also confirmed nearly complete elimination of CAR2 (Figure 4F). Furthermore, retinal flat-mounting and RGC staining were performed on DBA/2J mice at the fifth, ninth, and 10th months as well as on those injected with the AAVs (Figure 4G). The results revealed a progressive exacerbation of RGC loss with advancing age, whereas *Car2* KO demonstrated the ability to retard or even halt this phenomenon (Figures 4H and 4I).

Superior therapeutic potential of *Car2* KO over drug treatment in experimental glaucoma models

To further investigate the potential of *Car2* disruption as a therapeutic option for glaucoma, a chronic ocular hypertension (COH) mouse model was established by intracameral injection of magnetic microspheres (Figure S5A). During the first week of significantly elevated IOP, mice were randomly assigned to the COH group, COH+CAI group (brinzolamide eyedrop, twice a day), or COH+AAV group (single injection of AAVs), while contralateral eyes served as the control group for calculating binocular IOP difference (Figure 5A). Figure 5B illustrates a significant reduction in binocular IOP difference in both the brinzolamide-treated group and AAV-treated group compared to the COH group. Besides, the COH+AAV group exhibited a greater reduction in IOP, although statistical significance was observed only in the third week (Table S3). Histological analysis revealed that high IOP in the COH group led to pronounced whole retinal thinning, particularly in the nerve fiber layer and ganglion cell layer, which can be delayed and prevented by both drug treatment and gene KO interventions (Figures 5C, 5F, and S5B). In addition, RGC loss could be prevented through reducing IOP, and the effect of *Car2* KO is somewhat superior to CAI, especially in the peripheral region (Figures 5D, 5G, and S5C). Transmission electron microscopy results of the optic nerve displayed a persistent and significant reduction in axon quantity with prolonged high IOP, while reducing IOP by inhibiting carbonic anhydrase or disrupting *Car2* could effectively delay the progression of glaucoma (Figures 5E, 5H, S6A, and S6B).

DISCUSSION

The specific KO of the *Car2* gene in the ciliary body using the dual-target CRISPR system is a promising gene therapy intervention for glaucoma. Our results indicate that a single intravitreal injection can induce a significant and sustained reduction in IOP and exhibit superior therapeutic potential than clinically available CAIs in delaying or even halting glaucomatous progression induced by prolonged high IOP. These findings are important, highlighting the potential of this gene therapy approach for all types of glaucoma patients, complementing more traditional pharmacological interventions.

CAR2 is a zinc-containing metalloenzyme distributed in both the ciliary process and retina, playing a predominant and efficient role in the regulation of IOP.[11,26,30,31] While inhibiting CAR2 is considered adequate for the therapeutic effect to take place, specific KO of *Car2* has been challenging due to several reasons: (1) the *Car2* gene is widely expressed in all major mammalian organs and participates in crucial biological processes, including CO_2 transport, regulation of pH homeostasis,

(E) At week 4, there was no significant difference in total retinal thickness between the control group and the *Car2* KO group (6 eyes per group). Error bars indicate SEM.

(F and G) Representative graphs and statistical analysis of scotopic ERG at 0.01, 3.0, and 10.0 cd s/m^2, dark-adapted Ops, and PhNR (6 eyes per group). Error bars indicate SEM. OP, oscillatory potential; PhNR, photopic-negative response.

See also Figures S2 and S4.

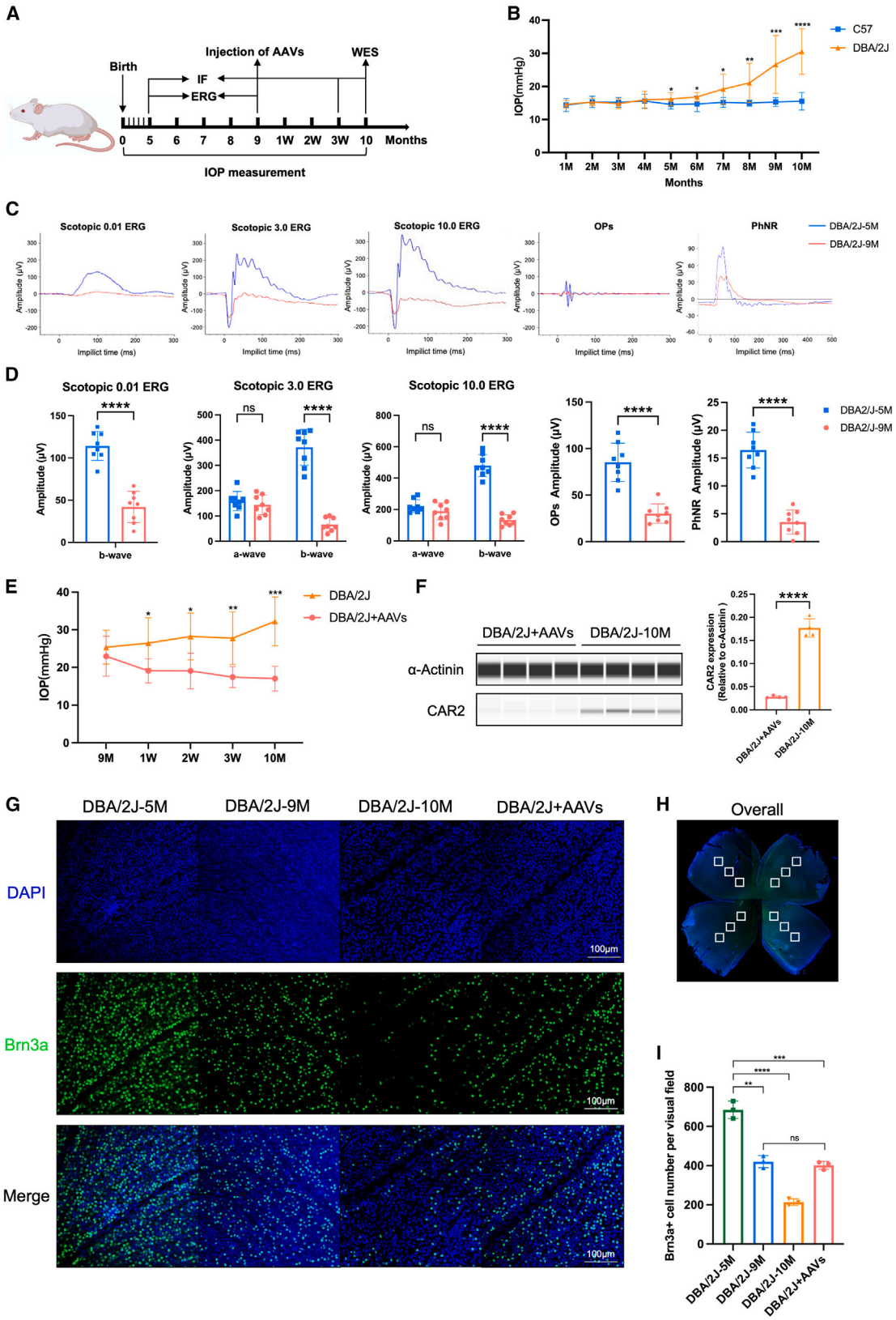

(legend on next page)

and bone resorption;[32–34] (2) "old drugs," like brinzolamide and dorzolamide, still dominate the glaucoma therapy landscape, with the majority of patents and published literature focusing primarily on formulations and delivery systems;[15,35] and (3) *Car2*-deficient (*Car2*$^{-/-}$) mice display metabolic acidosis, impaired urine acidification, and abnormal intercalated cells, making them unsuitable for glaucoma research.[36–38] Therefore, there is an urgent need to develop a new approach to specifically inhibit *Car2* gene expression in the ciliary body if this approach is to be used in the treatment of glaucoma.

RNA interference (RNAi) technology has been extensively employed for the knockdown of *Car2*,[39–41] which can silence gene expression in a sequence-specific manner. However, the clinical translation of RNAi-based therapy has proven challenging due to the RNA stability, delivery, endosomal escape, and off-target effects.[42] In contrast, CRISPR-Cas9 technology has emerged as a simple, efficient, and very specific genome editing tool compared with other genome editing techniques.[43] There is a growing body of evidence showing the promise of this approach in treating glaucoma via the disruption of the mutant myocilin gene (the first causative gene associated with glaucoma),[23] aquaporin 1,[24] and tumor growth factor β2.[44] To our knowledge, there is no published data on the use of CRISPR-Cas9 to disrupt the *Car2* gene and suppress protein function with a view to treating glaucoma or other diseases. In our study, the dual-target CRISPR system was able to significantly disrupt the *Car2* gene and reduce protein expression in mice. Disruption of exons 3 and 4 of the *Car2* gene using CRISPR-Cas9-mediated genome editing significantly reduced *Car2* mRNA expression. Although speculative, disruption of exons 3 and 4 could result in splicing errors and the production of aberrant mRNA molecules that get degraded by nonsense-mediated mRNA decay or alternatively interfere with its ability to be translated into a stable protein.

IOP reduction is a surrogate outcome to quantify intervention effectiveness,[45,46] and randomized trials have consistently shown that a 20% reduction in IOP from baseline halved the 5-year rate of glaucoma onset in the Ocular Hypertension Treatment Study,[47] and a 25% reduction significantly delayed glaucoma progression in the Early Manifest Glaucoma Trial.[48] However, in the present study, the suppression of *Car2* mediated by the dual-target CRISPR system led to an average 18% reduction in normal mice and 40% reduction in glaucoma model mice, which is comparable to the decrease in IOP previously reported with disruption of *aquaporin 1*[24] or mutant *myocilin*.[23] Crucially, the glaucomatous damage from the elevated IOP could be delayed or even halted by the KO of *Car2* gene. We were unable to use ERG and OCT as outcome measures in the magnet-induced COH model due to technical difficulties induced by interference from the magnetic beads.

Conventional CAIs, as topical anti-glaucoma medications, require daily instillation, and as they are often combined with other IOP-lowering medications,[35,49] adherence to treatment in a predominantly elderly population is far from satisfactory. Research is being focused on developing sustained drug delivery systems that can be positioned in the extraocular, periocular, and intraocular regions. The subconjunctival and intracameral delivery routes have both demonstrated a sustained and significant IOP-lowering effects of up to 2 years.[17] In contrast, the more routinely used intravitreal injection has not been widely explored as a route for sustained drug delivery.[17] The sustained IOP-lowering effect observed in our study with an intravitreal injection of AAVs is very encouraging. AAV-based delivery has a favorable immunogenic profile, and there is a low risk of serious complications, such as infection and vitreous hemorrhages.[49,50] Due to the possible transduction of the ShH10 serotype to the cornea and retina,[24] we investigated whether the disruption of *Car2* could have off-target effects in these tissues. Reassuringly, retinal histology and functional tests showed no side effects in the *Car2* KO mice, which is mainly because the disruption in the retina is incomplete, and other isoforms including Car14 are also present in the retina and still remain active.[51] No corneal swelling was observed in the *Car2* KO mice, which is consistent with the clinical experience of using traditional topical CAIs[52] or selective CAR2 inhibitors.[53]

The disruption of *Car2* in NPECs with CRISPR-Cas9 is an attractive therapeutic strategy for the management of all types of glaucoma by decreasing AH production.[54] However, further pre-clinical optimization is needed to assess the safety of this gene therapy approach and improve the efficacy *in vivo*. Both the ShH10 serotype derived from AAV6[55] and the AAV.7m8 variant derived from AAV2[56] are capable of transducing the ciliary body, but given the strong barriers to retinal transduction, other gene delivery systems, such as nanoliposomes, might also need to be considered.[57] Although the structure and protein function of CAR2 have been studied extensively,[58] undesirable repair events or genomic rearrangement after

Figure 4. Dual-target CRISPR system-mediated *Car2* KO lowers IOP in DBA/2J mice

(A) The experimental procedure involved monthly monitoring of IOP in DBA/2J mice from birth. ERG examinations were conducted at the fifth and ninth months. At the ninth month, a subset of DBA/2J mice received intravitreal injection of AAVs. Weekly IOP measurements were taken until the 10th month. Retinal flat-mounting and IF staining were performed at the fifth, ninth, and 10th months. Protein analysis was conducted on the AAV-treated group using WES.

(B) Monthly monitoring of IOP in 15 DBA/2J mice and 6 C57BL/6J mice from birth. Error bars indicate SEM. *$p < 0.05$, **$p < 0.01$, ***$p < 0.001$, ****$p < 0.0001$.

(C and D) Representative graphs and statistical analysis of scotopic ERG at 0.01, 3.0, and 10.0 cd s/m^2, dark-adapted Ops, and PhNR between the DBA/2J-5M and DBA/2J-9M groups (8 mice per group). Error bars indicate SEM. ****$p < 0.0001$.

(E) Weekly monitoring of IOP in the DBA/2J group and DBA/2J-AAV-treated group (8 eyes per group). Error bars indicate SEM. *$p < 0.05$, **$p < 0.01$, ***, $p < 0.001$.

(F) Expression and quantitative levels of *Car2* protein in the ciliary body of the DBA/2J group at the 10th month and DBA/2J-AAV-treated group were examined by WES (4 mice per group). Error bars indicate SEM. ****$p < 0.0001$.

(G) Representative retinal flat-mounting and IF staining of RGCs of the DBA/2J group at the fifth, ninth, and 10th months and the DBA/2J-AAV treated group.

(H) Schematic showing that two equidistant fields of the four leaflets of the retinal flat-mount were selected, and the average RGCs were calculated.

(I) RGC counting of the DBA/2J group at the fifth, ninth, and 10th months and the DBA/2J-AAV treated group (3 mice per group). Error bars indicate SEM. **$p < 0.01$, ***$p < 0.001$, ****$p < 0.0001$.

See also Figure S2.

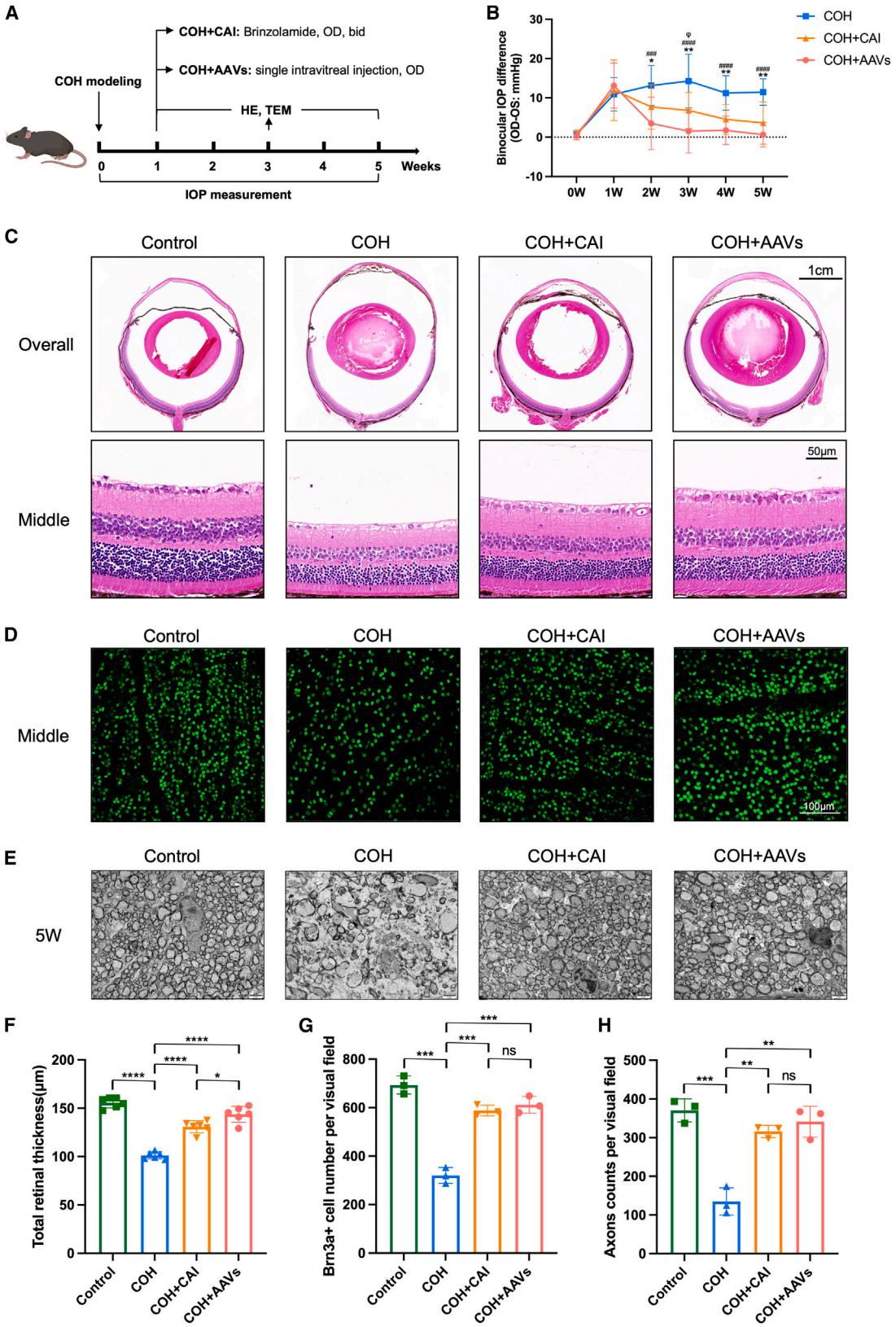

(legend on next page)

sgRNA-induced double-strand breaks cannot be ignored from a safety perspective.[43] Last, due to species-specific differences, a dual sgRNA system compatible for use in humans will need to be designed that effectively targets *Car2* expression, and this will require extensive evaluation for safety and gene editing efficiency.

Limitations of the study

While our findings are a promising step toward gene therapy for glaucoma, we must acknowledge some limitations in our study. First, the T7E1 assay could still be further optimized. When co-transfecting sgRNA3 and sgRNA5 *in vitro*, the bands after T7E1 enzyme digestion were not distinct, although there was a significant attenuation compared to the PCR products before digestion. Similarly, in *in vivo* experiments, the inability to precisely isolate the ciliary body may also lead to unclear bands after enzyme digestion due to tissue interference. Secondly, GUIDE-seq analysis confirmed that dual sgRNA-mediated gene editing did not increase off-target sites, but the *in vivo* situation remains unknown. We attempted to use primer extension-mediated sequencing to comprehensively and accurately quantify the DNA repair results;[59] however, due to the large amount of DNA samples required, the DNA extracted from mouse ciliary bodies was insufficient. Therefore, further exploration is needed in the pre-clinical safety assessment. Furthermore, the COH model induced by magnetic beads usually prevents us from performing OCT examinations and ERG functional assessments due to bead interference, so trying more models to further clarify the therapeutic effect of *Car2* KO could be beneficial.

Conclusion

The effective and specific disruption of *Car2* in the ciliary body was achieved through the utilization of a dual-target CRISPR system. Within a single intravitreal injection, this approach not only effectively reduces IOP but also showcases remarkable potential in significantly delaying or even halting the progression of glaucomatous damage. This transformative technique surpasses currently available CAIs in terms of efficacy, particularly considering that glaucoma can progress despite optimal medical and surgical interventions. Therefore, the application of CRISPR-Cas9 genome editing to modulate *Car2* gene expression represents a truly innovative approach, offering substantial hope for patients with glaucoma.

STAR★METHODS

Detailed methods are provided in the online version of this paper and include the following:

- KEY RESOURCES TABLE
- RESOURCE AVAILABILITY
  - Lead contact
  - Materials availability
  - Data and code availability
- EXPERIMENTAL MODEL AND STUDY PARTICIPANT DETAILS
  - Animal husbandry
  - Cell lines
- METHOD DETAILS
  - Design and construction of sgRNA and dual-sgRNA containing CRISPR-Cas9 plasmids
  - Sanger sequencing, deep sequencing and T7 endonuclease I (T7E1) assay
  - GUIDE-seq off-target assessment
  - AAV production and purification
  - Intravitreal injection
  - Microbead induced chronic ocular hypertension model
  - IOP measurement
  - Capillary-based immunoassay via ProteinSimple
  - Immunofluorescent imaging
  - Quantitative real-time PCR (qPCR)
  - Hematoxylin and eosin (H&E) and immunohistochemistry (IHC) staining
  - Spectral domain optical coherence tomography (SD-OCT)
  - Electroretinogram
  - Optic nerve section imaging under transmission electron microscope
  - Looming test
- QUANTIFICATION AND STATISTICAL ANALYSIS

SUPPLEMENTAL INFORMATION

Supplemental information can be found online at https://doi.org/10.1016/j.xcrm.2024.101524.

ACKNOWLEDGMENTS

This study was supported by the National Key Research and Development Program of China (2022YFC2502800); the National Natural Science Foundation of China (82070955 and 82101117); the Natural Science Foundation of Guangdong Province (2021A151501173); the Science and Technology Program of Guangzhou, China (202201020362); the National Institute for Health and Care Research (NIHR301696); the Rare Diseases Translational Research Collaboration, the NIHR Cambridge Biomedical Research Center (BRC-1215-20014); and Moorfields Eye Charity (GR001376). The authors thank

Figure 5. Comparison of *Car2* KO and CAI treatment in the experimental glaucoma model

(A) The experimental procedure involved weekly monitoring of IOP in the COH group, COH+CAI group, and COH+AAVs group. The H&E staining and transmission electron microscopy (TEM) were performed at the first, third and fifth weeks. COH, chronic ocular hypertension. CAI, carbonic anhydrase inhibitor.

(B) Binocular IOP difference of the COH group, COH+CAI group, and COH+AAVs group; the contralateral eyes served as the control group. *, COH vs. COH+CAI; #, COH vs. COH+AAVs; φ, COH+CAI vs. COH+AAVs (9 mice per group). Error bars indicate SEM. $^{*}p < 0.05$, $^{**}p < 0.01$, $^{***}p < 0.001$, $^{****}p < 0.0001$.

(C) H&E staining was performed at week 5, where the middle position was defined as 1.5 cm away from the optic disc, and the thickness of total retinal layers at this location was measured three times and averaged (6 eyes per group).

(D) Representative retinal flat-mounting and IF staining of RGCs using Brn3a; the average RGC counting was performed at the middle visual field (3 eyes per group).

(E) TEM of the optic nerve; the axon counting was performed at week 5 (3 eyes per group).

(F) Quantitative analysis of total retinal thickness (6 eyes per group). Error bars indicate SEM. $^{*}p < 0.05$, $^{****}p < 0.0001$.

(G) Quantitative analysis of Brn3a+ cell number per visual field (3 eyes per group). Error bars indicate SEM. $^{***}p < 0.001$.

(H) Quantitative analysis of axon counts per visual field (3 eyes per group). Error bars indicate SEM. $^{**}p < 0.01$, $^{***}p < 0.001$.

See also Figures S5 and S6.

the staff of the Core Facilities at the State Key Laboratory of Ophthalmology, Zhongshan Ophthalmic Center, for technical support and Wuhan Boerfu Biotechnology Co., Ltd., for help with IHC staining and TEM testing.

AUTHOR CONTRIBUTIONS

Conceptualization, F.L. and J.J.; methodology, J.J., K.K., and X.F.; investigation, J.J., X.F., K.K., D.W., Yinhang Zhang, Z.Y., Yuwei Zhang, and X.L.; visualization, J.J. and K.K.; funding acquisition, F.L. and X.Z.; project administration, F.L. and X.Z.; supervision, P.Y.-W.-M., T.A., and X.Z.; writing – original draft, J.J. and K.K.; writing – review & editing, P.Y.-W.-M., F.L., and X.Z.

DECLARATION OF INTERESTS

The authors declare no competing interests.

Received: November 2, 2023
Revised: February 27, 2024
Accepted: April 2, 2024
Published: April 25, 2024

REFERENCES

1. Jayaram, H., Kolko, M., Friedman, D.S., and Gazzard, G. (2023). Glaucoma: now and beyond. Lancet *402*, 1788–1801. https://doi.org/10.1016/S0140-6736(23)01289-8.
2. Stein, J.D., Khawaja, A.P., and Weizer, J.S. (2021). Glaucoma in Adults—Screening, Diagnosis, and Management: A Review. JAMA *325*, 164–174. https://doi.org/10.1001/jama.2020.21899.
3. Crowston, J.G., and Weinreb, R.N. (2005). Glaucoma medication and aqueous humor dynamics. Curr. Opin. Ophthalmol. *16*, 94–100. https://doi.org/10.1097/01.icu.0000156136.20570.eb.
4. Schuster, A.K., Erb, C., Hoffmann, E.M., Dietlein, T., and Pfeiffer, N. (2020). The Diagnosis and Treatment of Glaucoma. Dtsch. Arztebl. Int. *117*, 225–234. https://doi.org/10.3238/arztebl.2020.0225.
5. Dikopf, M.S., Vajaranant, T.S., and Edward, D.P. (2017). Topical treatment of glaucoma: established and emerging pharmacology. Expert Opin. Pharmacother. *18*, 885–898. https://doi.org/10.1080/14656566.2017.1328498.
6. Cvetkovic, R.S., and Perry, C.M. (2003). Brinzolamide: A Review of Its Use in the Management of Primary Open-Angle Glaucoma and Ocular Hypertension. Drugs Aging *20*, 919–947. https://doi.org/10.2165/00002512-200320120-00008.
7. Balfour, J.A., and Wilde, M.I. (1997). Dorzolamide. A review of its pharmacology and therapeutic potential in the management of glaucoma and ocular hypertension. Drugs Aging *10*, 384–403. https://doi.org/10.2165/00002512-199710050-00006.
8. Alterio, V., Di Fiore, A., D'Ambrosio, K., Supuran, C.T., and De Simone, G. (2012). Multiple Binding Modes of Inhibitors to Carbonic Anhydrases: How to Design Specific Drugs Targeting 15 Different Isoforms? Chem. Rev. *112*, 4421–4468. https://doi.org/10.1021/cr200176r.
9. Supuran, C.T. (2008). Carbonic anhydrases: novel therapeutic applications for inhibitors and activators. Nat. Rev. Drug Discov. *7*, 168–181. https://doi.org/10.1038/nrd2467.
10. Masini, E., Carta, F., Scozzafava, A., and Supuran, C.T. (2013). Antiglaucoma carbonic anhydrase inhibitors: a patent review. Expert Opin. Ther. Pat. *23*, 705–716. https://doi.org/10.1517/13543776.2013.794788.
11. Sugrue, M.F. (2000). Pharmacological and ocular hypotensive properties of topical carbonic anhydrase inhibitors. Prog. Retin. Eye Res. *19*, 87–112. https://doi.org/10.1016/S1350-9462(99)00006-3.
12. Mincione, F., Scozzafava, A., and Supuran, C.T. (2008). The development of topically acting carbonic anhydrase inhibitors as antiglaucoma agents. Curr. Pharm. Des. *14*, 649–654. https://doi.org/10.2174/138161208783877866.
13. Shalaby, W.S., Shankar, V., Razeghinejad, R., and Katz, L.J. (2020). Current and new pharmacotherapeutic approaches for glaucoma. Expert Opin. Pharmacother. *21*, 2027–2040. https://doi.org/10.1080/14656566.2020.1795130.
14. Lanier, O.L., Manfre, M.G., Bailey, C., Liu, Z., Sparks, Z., Kulkarni, S., and Chauhan, A. (2021). Review of Approaches for Increasing Ophthalmic Bioavailability for Eye Drop Formulations. AAPS PharmSciTech *22*, 107. https://doi.org/10.1208/s12249-021-01977-0.
15. Supuran, C.T., Altamimi, A.S.A., and Carta, F. (2019). Carbonic anhydrase inhibition and the management of glaucoma: a literature and patent review 2013-2019. Expert Opin. Ther. Pat. *29*, 781–792. https://doi.org/10.1080/13543776.2019.1679117.
16. Scozzafava, A., and Supuran, C.T. (2014). Glaucoma and the applications of carbonic anhydrase inhibitors. Subcell. Biochem. *75*, 349–359. https://doi.org/10.1007/978-94-007-7359-2_17.
17. Kompella, U.B., Hartman, R.R., and Patil, M.A. (2021). Extraocular, periocular, and intraocular routes for sustained drug delivery for glaucoma. Prog. Retin. Eye Res. *82*, 100901. https://doi.org/10.1016/j.preteyeres.2020.100901.
18. Komáromy, A.M., Koehl, K.L., and Park, S.A. (2021). Looking into the future: Gene and cell therapies for glaucoma. Vet. Ophthalmol. *24*, 16–33. https://doi.org/10.1111/vop.12858.
19. Miller, P.E., and Eaton, J.S. (2021). Medical anti-glaucoma therapy: Beyond the drop. Vet. Ophthalmol. *24*, 2–15. https://doi.org/10.1111/vop.12843.
20. Demetriades, A.-M. (2011). Gene therapy for glaucoma. Curr. Opin. Ophthalmol. *22*, 73–77. https://doi.org/10.1097/ICU.0b013e32834371d2.
21. Amador, C., Shah, R., Ghiam, S., Kramerov, A.A., and Ljubimov, A.V. (2022). Gene Therapy in the Anterior Eye Segment. Curr. Gene Ther. *22*, 104–131. https://doi.org/10.2174/1566523221666210423084233.
22. Hu, X., Zhang, B., Li, X., Li, M., Wang, Y., Dan, H., Zhou, J., Wei, Y., Ge, K., Li, P., and Song, Z. (2023). The application and progression of CRISPR/Cas9 technology in ophthalmological diseases. Eye (Lond) *37*, 607–617. https://doi.org/10.1038/s41433-022-02169-1.
23. Jain, A., Zode, G., Kasetti, R.B., Ran, F.A., Yan, W., Sharma, T.P., Bugge, K., Searby, C.C., Fingert, J.H., Zhang, F., et al. (2017). CRISPR-Cas9–based treatment of myocilin-associated glaucoma. Proc. Natl. Acad. Sci. USA *114*, 11199–11204. https://doi.org/10.1073/pnas.1706193114.
24. Wu, J., Bell, O.H., Copland, D.A., Young, A., Pooley, J.R., Maswood, R., Evans, R.S., Khaw, P.T., Ali, R.R., Dick, A.D., and Chu, C.J. (2020). Gene Therapy for Glaucoma by Ciliary Body Aquaporin 1 Disruption Using CRISPR-Cas9. Mol. Ther. *28*, 820–829. https://doi.org/10.1016/j.ymthe.2019.12.012.
25. Buabeng, E.R., and Henary, M. (2021). Developments of small molecules as inhibitors for carbonic anhydrase isoforms. Bioorg. Med. Chem. *39*, 116140. https://doi.org/10.1016/j.bmc.2021.116140.
26. Ghorai, S., Pulya, S., Ghosh, K., Panda, P., Ghosh, B., and Gayen, S. (2020). Structure-activity relationship of human carbonic anhydrase-II inhibitors: Detailed insight for future development as anti-glaucoma agents. Bioorg. Chem. *95*, 103557. https://doi.org/10.1016/j.bioorg.2019.103557.
27. Jiang, F., and Doudna, J.A. (2017). CRISPR-Cas9 Structures and Mechanisms. Annu. Rev. Biophys. *46*, 505–529. https://doi.org/10.1146/annurev-biophys-062215-010822.
28. Fierro, J., DiPasquale, J., Perez, J., Chin, B., Chokpapone, Y., Tran, A.M., Holden, A., Factoriza, C., Sivagnanakumar, N., Aguilar, R., et al. (2022). Dual-sgRNA CRISPR/Cas9 knockout of PD-L1 in human U87 glioblastoma tumor cells inhibits proliferation, invasion, and tumor-associated macrophage polarization. Sci. Rep. *12*, 2417. https://doi.org/10.1038/s41598-022-06430-1.
29. Liu, K., Sun, B., You, H., Tu, J.-L., Yu, X., Zhao, P., and Xu, J.-W. (2020). Dual sgRNA-directed gene deletion in basidiomycete Ganoderma lucidum

using the CRISPR/Cas9 system. Microb. Biotechnol. *13*, 386–396. https://doi.org/10.1111/1751-7915.13534.

30. Wistrand, P.J., Schenholm, M., and Lönnerholm, G. (1986). Carbonic anhydrase isoenzymes CA I and CA II in the human eye. Invest. Ophthalmol. Vis. Sci. *27*, 419–428.
31. Goel, R., Murthy, K.R., Srikanth, S.M., Pinto, S.M., Bhattacharjee, M., Kelkar, D.S., Madugundu, A.K., Dey, G., Mohan, S.S., Krishna, V., et al. (2013). Characterizing the normal proteome of human ciliary body. Clin. Proteomics *10*, 9. https://doi.org/10.1186/1559-0275-10-9.
32. Sly, W.S., and Hu, P.Y. (1995). Human carbonic anhydrases and carbonic anhydrase deficiencies. Annu. Rev. Biochem. *64*, 375–401. https://doi.org/10.1146/annurev.bi.64.070195.002111.
33. Parkkila, S. (2000). An overview of the distribution and function of carbonic anhydrase in mammals. EXS *90*, 79–93. https://doi.org/10.1007/978-3-0348-8446-4_4.
34. Kivelä, A.J., Kivelä, J., Saarnio, J., and Parkkila, S. (2005). Carbonic anhydrases in normal gastrointestinal tract and gastrointestinal tumours. World J. Gastroenterol. *11*, 155–163. https://doi.org/10.3748/wjg.v11.i2.155.
35. Stoner, A., Harris, A., Oddone, F., Belamkar, A., Verticchio Vercellin, A.C., Shin, J., Januleviciene, I., and Siesky, B. (2022). Topical carbonic anhydrase inhibitors and glaucoma in 2021: where do we stand? Br. J. Ophthalmol. *106*, 1332–1337. https://doi.org/10.1136/bjophthalmol-2021-319530.
36. Pan, P., Leppilampi, M., Pastorekova, S., Pastorek, J., Waheed, A., Sly, W.S., and Parkkila, S. (2006). Carbonic anhydrase gene expression in CA II-deficient (Car2−/−) and CA IX-deficient (Car9−/−) mice. J. Physiol. *571*, 319–327. https://doi.org/10.1113/jphysiol.2005.102590.
37. Krishnan, D., Pan, W., Beggs, M.R., Trepiccione, F., Chambrey, R., Eladari, D., Cordat, E., Dimke, H., and Alexander, R.T. (2017). Deficiency of Carbonic Anhydrase II Results in a Urinary Concentrating Defect. Front. Physiol. *8*, 1108. https://doi.org/10.3389/fphys.2017.01108.
38. Hains, D.S., Chen, X., Saxena, V., Barr-Beare, E., Flemming, W., Easterling, R., Becknell, B., Schwartz, G.J., and Schwaderer, A.L. (2014). Carbonic anhydrase 2 deficiency leads to increased pyelonephritis susceptibility. Am. J. Physiol. Renal Physiol. *307*, F869–F880. https://doi.org/10.1152/ajprenal.00344.2014.
39. Annan, D.A., Maishi, N., Soga, T., Dawood, R., Li, C., Kikuchi, H., Hojo, T., Morimoto, M., Kitamura, T., Alam, M.T., et al. (2019). Carbonic anhydrase 2 (CAII) supports tumor blood endothelial cell survival under lactic acidosis in the tumor microenvironment. Cell Commun. Signal. *17*, 169. https://doi.org/10.1186/s12964-019-0478-4.
40. Meng, T., Huang, R., Jin, J., Gao, J., Liu, F., Wei, Z., Xu, X., Chang, Z., Lin, J., Ta, N., et al. (2021). A comparative integrated multi-omics analysis identifies CA2 as a novel target for chordoma. Neuro Oncol. *23*, 1709–1722. https://doi.org/10.1093/neuonc/noab156.
41. Strowitzki, M.J., Nelson, R., Garcia, M.P., Tuffs, C., Bleul, M.B., Fitzsimons, S., Navas, J., Uzieliene, I., Ritter, A.S., Phelan, D., et al. (2022). Carbon Dioxide Sensing by Immune Cells Occurs through Carbonic Anhydrase 2-Dependent Changes in Intracellular pH. J. Immunol. *208*, 2363–2375. https://doi.org/10.4049/jimmunol.2100665.
42. Sioud, M. (2020). RNA and CRISPR Interferences: Past, Present, and Future Perspectives. Methods Mol. Biol. *2115*, 1–22. https://doi.org/10.1007/978-1-0716-0290-4_1.
43. Sharma, G., Sharma, A.R., Bhattacharya, M., Lee, S.-S., and Chakraborty, C. (2021). CRISPR-Cas9: A Preclinical and Clinical Perspective for the Treatment of Human Diseases. Mol. Ther. *29*, 571–586. https://doi.org/10.1016/j.ymthe.2020.09.028.
44. Rayana, N.P., Sugali, C.K., Dai, J., Peng, M., Liu, S., Zhang, Y., Wan, J., and Mao, W. (2021). Using CRISPR Interference as a Therapeutic Approach to Treat TGFβ2-Induced Ocular Hypertension and Glaucoma. Invest. Ophthalmol. Vis. Sci. *62*, 7. https://doi.org/10.1167/iovs.62.12.7.
45. Chan, P.P.M., Larson, M.D., Dickerson, J.E., Mercieca, K., Koh, V.T.C., Lim, R., Leung, E.H.Y., Samuelson, T.W., Larsen, C.L., Harvey, A., et al. (2023). Minimally Invasive Glaucoma Surgery: Latest Developments and Future Challenges. Asia. Pac. J. Ophthalmol. *12*, 537–564. https://doi.org/10.1097/APO.0000000000000646.
46. Zhang, Y., Chen, W., Lin, T.P.H., Zhang, X., Lam, D.S.C., and Chen, W. (2023). Outcomes of Goniotomy With or Without Secondary Intraocular Lens Implantation in Pediatric Glaucoma Following Cataract Surgery: A Prospective Pilot Study. Asia. Pac. J. Ophthalmol. *12*, 444–450. https://doi.org/10.1097/APO.0000000000000637.
47. Gordon, M.O., Beiser, J.A., Brandt, J.D., Heuer, D.K., Higginbotham, E.J., Johnson, C.A., Keltner, J.L., Miller, J.P., Parrish, R.K., Wilson, M.R., and Kass, M.A. (2002). The Ocular Hypertension Treatment Study: baseline factors that predict the onset of primary open-angle glaucoma. Arch. Ophthalmol. *120*, 714–830, discussion 829-830. https://doi.org/10.1001/archopht.120.6.714.
48. Heijl, A., Leske, M.C., Bengtsson, B., Hyman, L., Bengtsson, B., and Hussein, M.; Early Manifest Glaucoma Trial Group (2002). Reduction of intraocular pressure and glaucoma progression: results from the Early Manifest Glaucoma Trial. Arch. Ophthalmol. *120*, 1268–1279. https://doi.org/10.1001/archopht.120.10.1268.
49. Lusthaus, J.A., and Goldberg, I. (2017). Brimonidine and brinzolamide for treating glaucoma and ocular hypertension; a safety evaluation. Expert Opin. Drug Saf. *16*, 1071–1078. https://doi.org/10.1080/14740338.2017.1346083.
50. Bennett, J. (2017). Taking Stock of Retinal Gene Therapy: Looking Back and Moving Forward. Mol. Ther. *25*, 1076–1094. https://doi.org/10.1016/j.ymthe.2017.03.008.
51. Ochrietor, J.D., Clamp, M.F., Moroz, T.P., Grubb, J.H., Shah, G.N., Waheed, A., Sly, W.S., and Linser, P.J. (2005). Carbonic anhydrase XIV identified as the membrane CA in mouse retina: strong expression in Müller cells and the RPE. Exp. Eye Res. *81*, 492–500. https://doi.org/10.1016/j.exer.2005.03.010.
52. Malikowski, T.M., Bosch, J.B., Min, S., Duffey, M.E., and Patel, S.P. (2014). Carbonic anhydrase inhibitors in corneal endothelial transport. Invest. Ophthalmol. Vis. Sci. *55*, 2652–2658. https://doi.org/10.1167/iovs.13-13534.
53. Hou, Z., Li, C., Liu, Y., Zhang, M., Wang, Y., Fan, Z., Guo, C., Lin, B., and Liu, Y. (2020). Design, synthesis and biological evaluation of carbohydrate-based sulphonamide derivatives as topical antiglaucoma agents through selective inhibition of carbonic anhydrase II. J. Enzyme Inhib. Med. Chem. *35*, 383–390. https://doi.org/10.1080/14756366.2019.1705293.
54. Lusthaus, J., and Goldberg, I. (2019). Current management of glaucoma. Med. J. Aust. *210*, 180–187. https://doi.org/10.5694/mja2.50020.
55. Klimczak, R.R., Koerber, J.T., Dalkara, D., Flannery, J.G., and Schaffer, D.V. (2009). A novel adeno-associated viral variant for efficient and selective intravitreal transduction of rat Müller cells. PLoS One *4*, e7467. https://doi.org/10.1371/journal.pone.0007467.
56. Li, F., Wing, K., Wang, J.-H., Luu, C.D., Bender, J.A., Chen, J., Wang, Q., Lu, Q., Nguyen Tran, M.T., Young, K.M., et al. (2020). Comparison of CRISPR/Cas Endonucleases for in vivo Retinal Gene Editing. Front. Cell. Neurosci. *14*, 570917. https://doi.org/10.3389/fncel.2020.570917.
57. Liu, C., Zhang, L., Liu, H., and Cheng, K. (2017). Delivery Strategies of the CRISPR-Cas9 Gene-Editing System for Therapeutic Applications. J. Control. Release *266*, 17–26. https://doi.org/10.1016/j.jconrel.2017.09.012.
58. Cabaleiro-Lago, C., and Lundqvist, M. (2020). The Effect of Nanoparticles on the Structure and Enzymatic Activity of Human Carbonic

Anhydrase I and II. Molecules *25*, 4405. https://doi.org/10.3390/molecules25194405.

59. Yin, J., Liu, M., Liu, Y., Wu, J., Gan, T., Zhang, W., Li, Y., Zhou, Y., and Hu, J. (2019). Optimizing genome editing strategy by primer-extension-mediated sequencing. Cell Discov. *5*, 18. https://doi.org/10.1038/s41421-019-0088-8.

60. Concordet, J.-P., and Haeussler, M. (2018). CRISPOR: intuitive guide selection for CRISPR/Cas9 genome editing experiments and screens. Nucleic Acids Res. *46*, W242–W245. https://doi.org/10.1093/nar/gky354.

61. Tsai, S.Q., Zheng, Z., Nguyen, N.T., Liebers, M., Topkar, V.V., Thapar, V., Wyvekens, N., Khayter, C., Iafrate, A.J., Le, L.P., et al. (2015). GUIDE-seq enables genome-wide profiling of off-target cleavage by CRISPR-Cas nucleases. Nat. Biotechnol. *33*, 187–197. https://doi.org/10.1038/nbt.3117.

STAR★METHODS

KEY RESOURCES TABLE

REAGENT or RESOURCE	SOURCE	IDENTIFIER
Antibodies		
Rabbit polyclonal anti-Car2	Abcam	Cat# ab191343; RRID:AB_2801505
Rabbit polyclonal anti-Alpha Actinin	Proteintech	Cat# 11313-2-AP; RRID:AB_2223815
Mouse monoclonal anti-GFAP	Abcam	Cat# ab279289; RRID:N/A
Rabbit monoclonal anti-BRN3A	Abcam	Cat# ab245230; RRID:AB_2916038
Rabbit monoclonal anti-CD3	Abcam	Cat# ab16669; RRID:AB_443425
Rabbit polyclonal anti-CD11b	Abcam	Cat# ab133357; RRID:AB_2650514
Rabbit monoclonal anti-CD19	Abcam	Cat# ab245235; RRID:AB_2895109
Rabbit polyclonal anti-CD45	Abcam	Cat# ab10558; RRID:AB_442810
Alexa Fluor 555-conjugated anti-rabbit IgG	Cell Signaling Technology	Car# 4413; RRID: AB_10694110
Bacterial and virus strains		
pUC57-Simple-gRNA	Addgene	RRID:Addgene_51306
ShH10 cap	Addgene	RRID:Addgene_64867
Chemicals, peptides, and recombinant proteins		
DAPI	Sigma Aldrich	Cat# D9542
Optical cutting temperature compound	Servicebio	Cat# G6059
ProLong Gold Antifade Mountant	Thermo Fisher Scientific	Cat# P36934
Triton X-100	Sigma Aldrich	Cat# T8787
Bovine serum albumin	Beyotime	Cat# ST023
2.5% glutaraldehyde	Servicebio	Cat# G1102
FAS eyeball fixative solution	Servicebio	Cat# G1109
EDTA antigen retrieval buffer	Servicebio	Cat# G1206
Dulbecco's-Modified Eagle Medium	Sigma-Aldrich	Cat# D6429
Lipofectamine 3000	Thermo Fisher Scientific	Cat# L3000008
Critical commercial assays		
DNeasy Blood & Tissue Kit	QIAGEN	Cat# 69504
TaKaRa minibest Universal RNA Extraction Kit	Takara	Cat# 9767
EnGen Mutation Detection Kit	New England BioLabs	Cat# E3321S
Q5 High-Fidelity DNA polymerase	New England BioLabs	Cat# M0491S
PureLink Rapid gel extraction kit	Thermo Fisher Scientific	Cat# K210025
BCA protein concentration determination kit	Biosharp	Cat# BL521A
12–230 kDa Separation Module	ProteinSimple	Cat# SM-W004
ChamQ Universal SYBR qPCR Master Mix	Vazyme	Cat# Q711-03
Hematoxylin-Eosin staining Kit	Servicebio	Cat# G1005
Diaminobenzidine (DAB) Detection Kit (Polymer)	ZSGB	Cat# PV-6000D
Experimental models: Cell lines		
Mouse: Neuro-2a cell	ATCC	Cat# CCL-131, RRID:CVCL_0045
Experimental models: Organisms/strains		
Mouse: DBA/2J	The Jackson Laboratory	Strain #:000671 RRID:IMSR_JAX:000671
Mouse: C57BL/6J Nifdc	SPF (Beijing) Biotechnology Co., Ltd.	Cat# C57 100
Oligonucleotides		
Primer for *Car2* exon2	This Paper	F:ATTGCCAATGGAGACCGGC R:GCTAAAAAGCCCGATGGATGT

(*Continued on next page*)

Continued

REAGENT or RESOURCE	SOURCE	IDENTIFIER
Primer for *Car2* exon3	This Paper	F:TGGTAGGAAGTCAGGACAATCT R:TCTACTCAGTATGGGCTGGATT
Primer for *Car2* exon4	This Paper	F:CCTCAGTGACTCCTACAGATTG R:GTGTTCCAGTGAACCAAGTGA
Primer for *Car2* exon3+4	This Paper	F:CTGTTGTCCAGCAGTTAGCACAT R:TGTTCCAGTGAACCAAGTGAAGC
Primer for CD3	This Paper	F:CCCTGAGTCCCCTCTACACTT R:TGCCCCAGAAAGTGTTCCAC
Primer for CD11b	This Paper	F:CCACACTAGCATCAAGGGCA R:AAGGGACACACTGACACCTG
Primer for CD19	This Paper	F:GGACAGTGAACGTGGAGGAT R:GGGCACATACAGGCTTTGTT
Primer for CD45	This Paper	F:ATGGTCCTCTGAATAAAGCCCA R:TCAGCACTATTGGTAGGCTCC
Primer for CAR2	This Paper	F:CAAGCACAACGGACCAGA R:ATGAGCAGAGGCTGTAGG
Primer for Gapdh	This Paper	F:CATGGCCTTCCGTGTTCCT R:GCCTGCTTCACCACCTTCT
Recombinant DNA		
ssAAV.U6.(Sp)sgRNA.CAG.SV40 NLS-EGFP.WPRE	Packgene	N/A
ssAAV.miniCMV.SpCas9	Packgene	N/A
Software and algorithms		
CRISPOR	Jean-Paul Concordet et al.[59]	http://crispor.tefor.net/crispor.py
GUIDE seq	Shengdar Q Tsai et al.[60]	http://jounglab.org/guideseq
Compass for SW software (V6.2.0)	Protein Simple	https://www.proteinsimple.com/compass/downloads/
ImageJ	ImageJ	https://imagej.net/ij/download.html
Prism 10.2.1	GraphPad software	https://www.graphpad.com/updates

RESOURCE AVAILABILITY

Lead contact

Further information and requests for resources and reagents should be directed to and will be fulfilled by the lead contact, Xiulan Zhang (zhangxl2@mail.sysu.edu.cn).

Materials availability

This study did not generate new materials.

Data and code availability

- All data reported in this paper will be shared by the lead contact upon request.
- This paper does not report original code.
- Any additional information required to reanalyze the data reported in this paper is available from the lead contact upon request.

EXPERIMENTAL MODEL AND STUDY PARTICIPANT DETAILS

Animal husbandry

Adult (six to eight weeks old) C57BL/6J female mice were purchased from the SPF (Beijing) Biotechnology Co., Ltd. and housed at the Animal Laboratory of Zhongshan Ophthalmic Center (Guangzhou, China) in a 12-h light/dark cycle (lights on from 6:00 a.m. to 6:00 p.m.) with food and water *ad libitum*. The DBA/2J strain was procured from the Jackson Laboratory in the United States and subsequently maintained through a breeding program to ensure its genetic stability. All animal procedures were approved by the Institutional Animal Care and Use Committee of Zhongshan Ophthalmic Center. All animal cares and experimentations complied with the Association for Research in Vision and Ophthalmology Statement for the Use of Animals in Ophthalmic and Vision Research.

Cell lines

Neuro-2a (N2a) cells were purchased from ATCC (CCL-131) and cultured in growth media consisting of Dulbecco's-Modified Eagle Medium (DMEM, Sigma-Aldrich, D6429) supplemented with 10% v/v heat-inactivated fetal bovine serum, 100 U/mL penicillin, and 100 mg/mL streptomycin (all from Thermo Fisher Scientific) at 37°C with 5% CO2. Cells were co-transfected with a 2μg plasmids containing a 1:1 ratio of sgRNA-expressing plasmid and a SpCas9-expressing plasmid (Packgene Biotech, China) using the Lipofectamine 3000 (Thermo Fisher Scientific, L3000008) protocol. Cells treated with only 2μg SpCas9-expressing plasmid served as control in all cell experiments.

METHOD DETAILS

Design and construction of sgRNA and dual-sgRNA containing CRISPR-Cas9 plasmids

Mouse *Car2* genomic sequence was obtained from the *Ensemble* database, and the sequences of exon 2, 3 and 4 from the most functional transcript *Car2*-201 (ENSMUST00000029078.9) were loaded onto the CRISPOR online-tool[60] (http://crispor.tefor.net/crispor.py). Through the evaluation of the specificity and predicted off-target mismatches, we designed and selected two candidate sgRNAs for each exon. Plasmid construction was commissioned from Packgene Biotech in China. SgRNA expression under control of the human U6 promoter was synthesized and cloned into the SapI site of ssAAV.U6.(Sp)sgRNA.CAG.SV40 NLS-EGFP.WPRE (Packgene, ssAAV-EA021-100). The Cas9 expression vector was purchased from Packgene Biotech (ssAAV.miniCMV.SpCas9, AAV-XB06) which has a miniCMV promoter that drives expression of Cas9. For the dual sgRNA based CRISPR-Cas9 plasmid, the U6-sgRNA3-U6-sgRNA5 was synthesized and cloned into the EcoRV site of pUC57-Simple vector (Addgene_51306). The dsDNA fragment was amplified using the forward primer of TGTAAAACGACGGCCAGT and reverse primer of CAGGAAACAGCTATGACC, which was then cloned into the MluI and SalI-digested ssAAV vector mentioned above. Finally, the plasmid ssAAV-sgRNA3-sgRNA5-EGFP was prepared for the virus packaging.

Sanger sequencing, deep sequencing and T7 endonuclease I (T7E1) assay

The genomic DNA were extracted from the transduced cells and tissues using the DNeasy Blood & Tissue Kit (QIAGEN, 69504) following the manufacturer's protocol and amplified with primers bracketing the modified locus using Q5 High-Fidelity DNA polymerase (New England BioLabs, M0491S). The PCR products were separated in 2% agarose gel and purified with a gel extraction kit (Thermo Fisher Scientific, K210025) for Sanger DNA sequencing and deep sequencing with the 10,000 reads.

For T7E1 assay, the PCR products were checked on an agarose gel (primers were listed in the Key resources table), and then the samples were denatured for 10 min at 95°C and allowed to cool slowly to room temperature in order to allow formation of heteroduplex with and without mutations. Finally, the sample was digested with the EnGen Mutation Detection Kit (New England BioLabs, E3321S) for 15 min at 37°C followed by Proteinase K digestion for 5 min at 37°C, and the resulting products were analyzed by agarose gel electrophoresis.

GUIDE-seq off-target assessment

The GUIDE-seq library construction and sequencing steps were the same as described in previous study by GeneRulor (zhuhai).[61] Briefly, genomic DNA was randomly fragmented to 500bp by Bioruptor pico (Diagenode) ultra-sonication. Adapters were ligated to the end-repaired DNA, and then two rounds of PCR were performed to amplify the sequence carrying dsODN tag. The library was sequenced on MGI 2000 platform with 150-bp paired-end reads. Data was analyzed using open-source GUIDE seq software (http://jounglab.org/guideseq).

AAV production and purification

The AAV was packaged by Packgene Biotech in China. Triple-plasmid transfection using the polyethylenimine (PEI, Polysciences) was carried out to produce the recombinant AAV. The plasmid ssAAV-sgRNA3-sgRNA5-EGFP described in the previous sgRNA design section, pHelper, and plasmid encoding the ShH10 capsid protein (Addgene_64867) were co-transfected into HEK293T cells. The ShH10 particles were further purified and concentrated by column chromatography on a 1-mL HiTrap AVB Sepharose column (GE Healthcare, USA) and eluted with 50 mM glycine (pH 2.7) into 1 M Tris (pH 8.8). Vector-containing fractions were then concentrated and buffer exchanged in PBS-MK to a concentration of 1×10^{13} genome copies per milliliter (gc/mL) using a Vivaspin 4 (10 kDa) concentrator. Vector was then titered for DNase-resistant vector genomes by real-time PCR relative to a standard. Finally, the purity of the vector was validated by silver-stained sodium dodecyl sulfate–polyacrylamide gel electrophoresis, assayed for sterility and lack of endotoxin, and then aliquoted and stored at −80°C.

Intravitreal injection

Intravitreal injections were performed under the operating microscope. Mice were anesthetized with an intraperitoneal injection of pentobarbital sodium (50 mg/kg), pupils were dilated with 1% atropine sulfate and topical anesthesia were achieved using one drop of 0.5% proparacaine hydrochloride. Then, a 2μL ShH10-based AAVs (a 1:1 mixture of ssAAVShH10-sgRNA3-sgRNA5-EGFP and ssAAVShH10-miniCMV-SpCas9) were injected using a 5μL microinjector (Hamilton, Reno, NV) fitted with a 33-gauge needle. Tobramycin ointment was applied to the ocular surface after surgery.

Microbead induced chronic ocular hypertension model

After anesthesia and pupil dilation (as previously described for intravitreal injection), the anterior chamber was cannulated by using a 32-gauge needle inserted through the corneal limbus at an angle, taking care not to damage the iris. The needle was pulled out to allow outflow of AH and an appropriate amount of air was injected with a 5μL micro-syringe equipped with a 32-gauge needle to create small air bubbles for subsequent magnetic microspheres distribution. Afterward, a 10-μL micro-syringe equipped with a 32-gauge needle was used to inject 6μL of magnetic microspheres (Bangs Laboratories, Fishers, IN, United States; diameter: 10 μm; diluted concentration: 25 mg/mL) at the same puncture point. The magnetic microspheres were sucked with a magnet on the opposite side of the needle entry point, and then a strong neodymium circular magnet ring (3mm in diameter) was used to evenly suck the magnetic microspheres to the anterior chamber angle. Tobramycin ointment was applied on the eye surface after surgery. Then the animals were placed on absorbent paper atop a 37°C heating plate for recovery and placed back in their cages after natural awakening.

IOP measurement

Mice were anesthetized by intraperitoneal injection (as previously described for intravitreal injection) and IOP was measured 5 min later, using a TonoLab rebound tonometer (Icare, Vantaa, Finland) according to the manufacturer's instructions. IOP measurements were performed between 14:00 and 17:00 Beijing Standard Time. Eyes were alternately tested 5 min after introduction of anesthesia. The mean of three successful measurements from each eye was recorded for analysis, and each measurement included the average of six rebound tests. Paired eyes were tested alternately to control for the effect of anesthesia on IOP.

Capillary-based immunoassay via ProteinSimple

For CAR2 expression analysis, the ProteinSimple capillary-based immunoassay was performed on a Wes system (Abby, ProteinSimple, San Jose, CA) according to the manufacturer's instructions using a 12–230 kDa Separation Module (ProteinSimple SM-W004). In brief, the cornea, ciliary body and retina were carefully isolated, and placed in lysis solution (0.1 M Tris, pH 7.4, 1 mM EDTA) to extract the proteins. Protein concentrations were determined by the bicinchoninic acid (BCA) method (Biosharp, BL521A) and diluted to an appropriate concentration (3 μg/mL of the cornea, 1 μg/mL of the ciliary body and 0.5 μg/mL of the retina) in sample buffer. According to the manufacturer's protocol, primary antibodies against the CAR2 (Abcam, ab191343) and α-Actinin (Proteintech, 11313-2-AP) were diluted to the following concentrations: 1:10 and 1:5000 for cornea, 1:50 and 1:10000 for ciliary body, 1:100 and 1:1000 for retina, respectively. Antibody targets were detected with an HRP-conjugated secondary anti-rabbit antibody (ProteinSimple DM-001). Digital images were analyzed using Compass for SW software (V6.2.0, Protein Simple, https://www.proteinsimple.com/compass/downloads/) and quantified data were exported.

Immunofluorescent imaging

For EGFP, CAR2 and GFAP immunofluorescent imaging, mouse eyes were fixed with 4% paraformaldehyde, frozen in optical cutting temperature compound (Servicebio, G6059), and sectioned at 14-μm intervals. Slides were incubated with a 1:200 dilution of anti-CAR2 (Abcam, ab191343) or anti-GFAP antibody (Abcam, ab279289) over night, followed by secondary antibody Alexa Fluor 555-conjugated anti-rabbit/mouse IgG (Cell Signaling Technology, 4413S/4409S) and DAPI (Sigma Aldrich, D9542), finally mounted in fluorescence mounting media (Thermo Fisher Scientific, P36934) before imaging on an inverted fluorescence microscope (Nikon Eclipse Ni-U; Nikon, Tokyo, Japan) or laser confocal microscope (LSM 800, Zeiss, Germany).

For RGCs specific immunofluorescent staining, retinal cryosections and retinal flat mount were performed. In brief, retina was blocked with 1% Triton X-100 (Sigma Aldrich, T8787) and 3% bovine serum albumin (BSA, Beyotime, ST023) buffer for 1 h at room temperature. A specific RGCs marker, anti-BRN3A antibody (Abcam, ab245230) was used to incubate overnight at 4°C, followed by secondary antibody Alexa Fluor 488-conjugated anti-rabbit IgG (Cell Signaling Technology, 4412S) and DAPI (Sigma Aldrich, D9542). Images were captured with an inverted fluorescence microscope (Nikon Eclipse Ni-U; Nikon, Tokyo, Japan) or laser confocal microscope (LSM 800, Zeiss, Germany). The RGCs density in the same position (1–2 mm from the optic disc) of both groups were calculated in corresponding with retinal length or area measured using ImageJ software (https://imagej.net/ij/download.html).

Quantitative real-time PCR (qPCR)

RNA was extracted from ciliary body using TaKaRa minibest Universal RNA Extraction Kit (Takara, 9767) and quantified with NanoDrop One/OneC (Thermo Scientific, USA). Quantitative real-time PCR was carried out in triplicates on a Light Cycler 480 II (Roche, Switzerland) using ChamQ Universal SYBR qPCR Master Mix (Vazyme, Q711-03). Gapdh values were used for data normalization. The primers utilized are listed in the Key resources table.

Hematoxylin and eosin (H&E) and immunohistochemistry (IHC) staining

Eyes were enucleated and fixed in FAS eyeball fixative solution (Servicebio, G1109) embedded in paraffin, and sectioned at 6 μm thickness. H&E staining of retinal sections was performed using a Hematoxylin-Eosin staining Kit (Servicebio, G1005). For IHC staining, sections were dewaxed, rehydrated, and then retrieved using EDTA antigen retrieval buffer (Servicebio, G1206) followed by blocking with 10% normal goat serum. After incubation with primary antibodies overnight at 4°C, the sections were incubated

with horseradish peroxidase-conjugated anti-rabbit IgG antibody (ZSGB, PV-6000D), followed by Diaminobenzidine (DAB) Detection Kit (Polymer) (ZSGB, PV-6000D) and hematoxylin (Servicebio, G1004). The primary antibodies are outlined in the key sources table.

Spectral domain optical coherence tomography (SD-OCT)

After anesthesia and pupil dilation (as previously described for intravitreal injection), mice were positioned correctly, and OCT scans were taken automatically with a quality index of over 28 using SPECTRALIS-OCT system Heidelberg, Germany). ImageJ software to measure and analyze the thickness of the retina.

Electroretinogram

Electroretinograms (ERG) was performed following dark adaptation of the mice overnight, the pupils were dilated using 0.5% phenylephrine and 0.5% tropicamide eye drops under deep anesthesia (pentobarbital sodium, 70 mg/kg). The scotopic flash ERG was recorded using a series of white flashes (0.003, 0.01, 0.03, 0.1, 0.3, 1, 3 and 10 cd s/m^2) under dark adaptation and subsequent analysis focused on evaluating the amplitudes of the a-wave, b-wave, and oscillatory potentials (OPs). After the scotopic flash ERG, the mice were subjected to a 10-min adaptation period under a blue light background. Subsequently, the absence of a negative wave response known as the photopic negative response (PhNR) was recorded using a stimulation light intensity of 10.0 cd s/m^2.

Optic nerve section imaging under transmission electron microscope

Optic nerve was dissected and fixed with 2.5% glutaraldehyde (Servicebio, G1102) and ultrathin sections (80 nm) of the optic nerve segments were collected. Each section was examined under a transmission electron microscope (TEM, HT7800, HITACHI, Japan). The assessment of axon was quantitatively calculated and analyzed.

Looming test

In a standardized arena setting, the defensive behaviors elicited by looming visual stimuli was quantified. Computer monitor positioned above the stage aims to present faint visual stimuli using a gradually expanded dark disc. Upon entering the arena, the mice were allowed a 10-min period of exploration. The latency period for the mice to return to their nest after the stimulus was recorded as an indicator of defensive response.

QUANTIFICATION AND STATISTICAL ANALYSIS

All data were presented as mean ± standard deviation (SD). Statistical analyses were performed using one-way ANOVA or two-tailed Student's t test, $p < 0.05$ was considered significant. Prism 10.2.1 GraphPad software (GraphPad Software, CA) was used to analysis and draw graphs. ImageJ software (NIH, Bethesda, MA, USA) was used to quantitative analysis the loss of RGCs and axons.